Int. J. Solids Structures Vol. 29, No. 20, pp. 2493–2502, 1992
Printed in Great Britain.

0020-7683/92 $5.00 + .00

THE EFFECT OF INTERFACE ON THE TRANSVERSE PROPERTIES OF COMPOSITES

J. R. YEH
Aluminum Company of America, Alcoa Laboratories, Alcoa Center, PA 15069, U.S.A.

(*Received* 17 *December* 1990; *in revised form* 5 *February* 1992)

Abstract—The effect of interface bond strength on the transverse behavior of elastic–plastic composite materials is studied. A finite element model employing special interface elements is developed for this study. The interface element allows modeling of either perfect bonding or debonding based on the interfacial stress state. The results of this study provide detailed information regarding the failure mechanisms and the ultimate strength of fiber-reinforced materials. Numerical examples are presented for a Kevlar/epoxy composite system. Failure envelopes for the composite under biaxial loading are obtained for various interface bond strengths. The numerical results are in good agreement with the experimental data.

1. INTRODUCTION

The inclusion of fibers in a matrix is frequently used to produce a composite material with more desirable mechanical properties than either material alone. Design values for mechanical properties are normally obtained from laboratory tests. In fact, laboratory and field load tests give valuable and, to a significant degree, analytically indeterminable information on the behavior of fiber-reinforced materials. However, the ability to judge the probable response of such materials to untested loading conditions, or to rationally modify the design of such materials to improve their mechanical response requires knowledge of the micromechanical interactions of the constituent materials.

The ability of the bond between fiber and matrix to transfer load across the interface strongly affects the mechanical response of composite materials. The objective of this study is to devise and verify a method of analysis which may be used to investigate the micromechanical interfacial debonding mechanisms of a class of fiber-reinforced materials, consisting of an isotropic, elastic–plastic matrix containing transversely isotropic, linearly elastic fibers. The material is loaded in the direction normal to the fiber axis.

Perhaps the most widely used analytical approach for estimating the properties of composite materials is the rule of mixtures, which can reasonably predict the Young's and shear moduli of the composites when the composite has a very strong bond between fiber and matrix. However, the rule of mixtures technique does not apply well to failure properties because it fails to account for the stress concentration which results from the fiber/matrix interactions. Many other models have beeen developed by Hill (1964), Adams and Tsai (1969), Hashin (1979), Chou *et al.* (1980), Oshima and Nomura (1985), Takahashi and Chou (1988) and Teply and Dvorak (1988) to predict the mechanical behavior of composite materials; all of them assume either perfect bonding or debonding at the fiber/matrix interface. No attempt was made in the models to include a failure criterion for interfacial debonding during the loading history.

In this study, the effect of the interface bond strength on the transverse response of elastic–plastic composite materials is investigated. A binary periodic microstructure subjected to macroscopically uniform stress is considered. A unit cell of the periodic microstructure is subdivided into regular and interface elements; the interface elements are developed to model either perfect bonding or debonding based on the present interfacial stress state. The solutions of local stress and strain fields and overall properties are obtained using the finite element technique.

In the next section, the unit cell which represents the composite's periodic microstructure is addressed. In Section 3, the finite element model and the development of an interface element for evaluating the local fields and overall properties of the composite are

described. Finally, the influence of interface bond strength on the transverse properties of the Kevlar/epoxy composite system is demonstrated and discussed. The numerical results are compared with experimental data whenever possible.

2. GEOMETRY OF THE PERIODIC MICROSTRUCTURE

Although composite microstructures are random, periodic distributions of fibers in a matrix are often assumed, especially for composites with high fiber volume fractions. Evaluation of the overall properties of a binary composite is performed on a small unit cell, which represents the periodic microstructure. The unit cell for the Periodic Hexagonal Array (PHA) model was developed and used by Teply and Dvorak (1988) to estimate instantaneous local stress and strain fields, and the overall moduli of elastic–plastic composites. This unit cell is expanded in this study and applied to problems of bonding/debonding at the fiber/matrix interface in binary composites. A detailed discussion of the concepts of the PHA model is given in Teply and Dvorak (1988). Only relationships relevant to the current problem are given below.

For composites reinforced by aligned continuous fibers, the problem may be treated as a generalized plane strain problem. Figure 1 shows a transverse section of the composite with fiber placed in a regular periodic hexagonal array. The fibers are assumed to have identical circular cross-sections. The unit cell can be chosen as a triangle with vertices at adjacent fiber centers. There are two sets of such triangular cells, indicated by shaded and unshaded triangles in Fig. 1. It has been shown in Teply and Dvorak (1988) that either cell can be generated through rotation of the properties associated with the other cell.

Under overall uniform transverse stresses, the deformation of the composite unit cell can be compared to that of an effective homogeneous unit cell, which has the same overall properties of the composite. In particular, it is possible to identify certain contact points in both the composite and homogeneous cells which experience exactly the same displacements under uniform overall loading. For the geomery shown in Fig. 1, any macroscopically uniform deformation of the composite can be specified in terms of relative displacements of the fiber centers, and therefore the vertices of the triangular unit cell are chosen as contact points.

3. EVALUATION OF THE LOCAL AND OVERALL PROPERTIES

3.1. *Finite element model*

The local fields and overall properties of the unit cell are evaluated from the displacement formulation of the finite element method. The equilateral triangle unit cell is

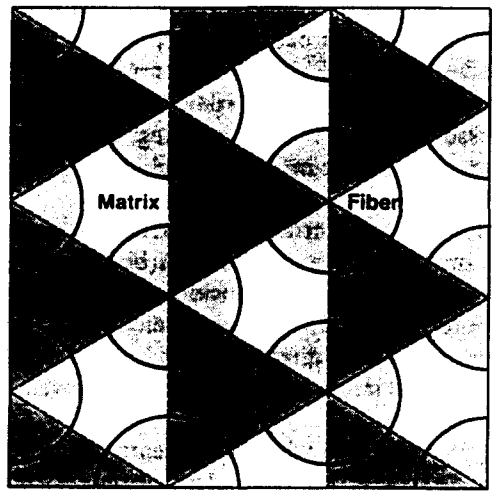

Fig. 1. Transverse section of periodic hexagonal array model of binary composites.

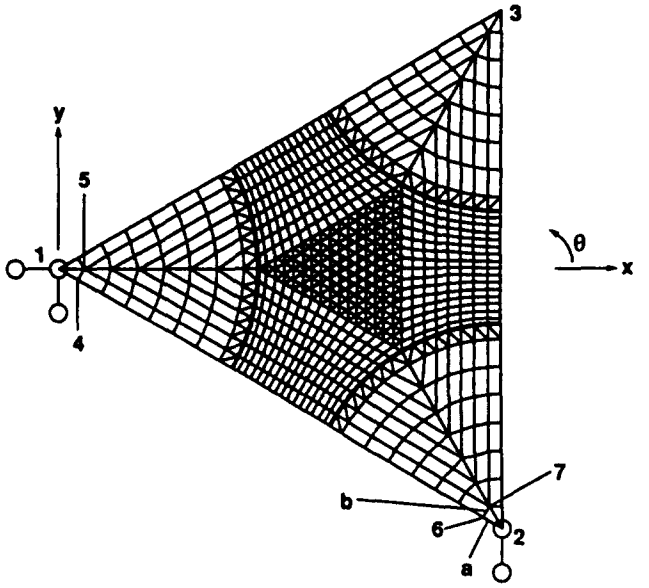

Fig. 2. Finite element mesh for the equilateral triangle unit cell.

divided into finite elements as shown in Fig. 2. The relative areas of the fiber and matrix are determined from the fiber volume fraction. Three- and four-node generalized plane strain elements are used to discretize the regions. Adjacent elements in the fiber and matrix are connected by interface elements, which will be discussed in the next section.

The large-strain theory and one point integration scheme are used to calculate the element stiffness matrix. For the complexities of the occurrence of debonding and the material inelasticity, the technique of the incremental loading path is used in the analysis. Two distinct groups of constraint conditions are introduced to meet the compatibility and equilibrium requirements at the boundary of the unit cell. These requirements need to be satisfied at each increment. Examples of each of these constraint conditions are discussed in the following sections.

(a) *Compatibility requirement.* In order to maintain compatibility between adjacent unit cells, the sum of the relative displacement of node 4 to node 1 and the relative displacement of node 6 to node 2 should be equal to zero (see Fig. 2), i.e.

$$u_4-u_1+u_6-u_2=0, \qquad v_4-v_1+v_6-v_2=0, \tag{1,2}$$

where u and v denote the displacements in the x- and y-directions, respectively.

(b) *Equilibrium requirement.* According to the requirement of traction equilibrium at adjacent nodes, the shear strain and the strain normal to the surface at node 4 should be equal to the corresponding strains at node 6, i.e.

$$(U_4-U_5)/a=(U_6-U_7)/a, \qquad (U_4-U_1)/b+(V_4-V_5)/a=(U_2-U_6)/b+(V_6-V_7)/a, \tag{3,4}$$

where a and b are the sizes of the element shown in Fig. 2; U and V are the displacements normal and parallel to the surface, respectively. By a simple transformation, U and V can be related to u and v as follows:

$$U=u\cos\theta+v\sin\theta, \qquad V=-u\sin\theta+v\cos\theta, \tag{5,6}$$

where θ is the angle measured counterclockwise from the x-axis to the normal direction of

the surface. Substituting eqns (1), (2), (5) and (6) into eqns (3) and (4), the boundary conditions for the equilibrium requirement can be rewritten as:

$$u_4 - u_5 = u_6 - u_7, \qquad v_4 - v_5 = v_6 - v_7. \tag{7,8}$$

Therefore, eqns (1), (2), (7) and (8) are the constraint equations for nodes 4 and 6. Similar constraint equations are obtained for the other nodes on the boundary of the unit cell. Note that constraint equations can be written for all nodal degrees of freedom on the boundary except those at the vertices of the unit cell.

3.2. *Development of the interface element*

The basic function of the interface element can be described as follows. The normal and shear stresses along the interface are estimated under the condition of perfect bonding between the fiber and matrix. These stresses are compared to the allowable stresses (i.e. interfacial tensile and shear strengths). Debonding occurs when the estimated stresses exceed the allowable stresses. Note that in this study, the interfacial shear debonding is not considered, since the interfacial shear strength is usually much larger than the interfacial tensile strength. Therefore, the debonding will take place when the interfacial tensile stress exceeds the interfacial tensile strength. The process of debonding is modeled by setting the stiffness of the interface element to zero and therefore there are no normal nor shear stresses at the debonded interface.

The interface element developed here consists of four nodes with local node numbers illustrated in Fig. 3. Points A and B denote the ends of the interface element associated with local nodes $\{1,3\}$ and $\{2,4\}$, respectively. The coordinate axes and the convention for specifying the normal, n, and the tangent, t, to the interface are indicated in the figure. The normal and tangent components of the relative displacements, $\{U\}$, at the points A and B can be obtained from the nodal displacements, $\{u\}$:

$$\{U\} = [T]\{u\}, \tag{9}$$

where

$$\{U\} = \{U_A, V_A, U_B, V_B\}^T, \quad \{u\} = \{u_1, v_1, u_2, \ldots, v_4\}^T,$$

and

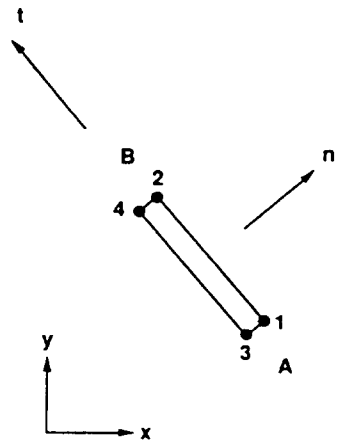

Fig. 3. Coordinates and node numbering for the interface element.

$$[T] = \begin{vmatrix} \alpha & \beta & 0 & 0 & -\alpha & -\beta & 0 & 0 \\ -\beta & \alpha & 0 & 0 & \beta & -\alpha & 0 & 0 \\ 0 & 0 & \alpha & \beta & 0 & 0 & -\alpha & -\beta \\ 0 & 0 & -\beta & \alpha & 0 & 0 & \beta & -\alpha \end{vmatrix}, \quad \text{with} \quad \alpha = \cos\theta, \quad \beta = \sin\theta,$$

and θ is the angle measured counterclockwise from the x-axis to the normal direction.

The interface element consists of springs between points A and B in both the normal and tangential directions. Two stiffness properties of the springs for the interface elements allow the displacements normal to the interface or tangential to the interface to be either continuous across the interface or allow the two adjacent materials to move independently. A continuous displacement (essentially infinite stiffness) in both directions stimulates a perfect bond condition. To model a location on the interface where a bond failure has occurred, both the normal and tangential stiffnesses are set to zero.

The forces at the nodes, $\{F\}$, can be determined as functions of the normal stiffness (k_n) and tangential stiffness (k_t) of the springs and $\{U\}$:

$$\{F\} = [Ki]\{U\}. \tag{10}$$

In the above equation,

$$\{F\} = \{F_{n1}, F_{t1}, F_{n2}, \ldots, F_{t4}\}^T,$$

and

$$[Ki] = \frac{L}{6} \begin{vmatrix} 2k_n & 0 & k_n & 0 & -2k_n & 0 & -k_n & 0 \\ 0 & 2k_t & 0 & k_t & 0 & -2k_t & 0 & -k_t \\ k_n & 0 & 2k_n & 0 & -k_n & 0 & -2k_n & 0 \\ 0 & k_t & 0 & 2k_t & 0 & -k_t & 0 & -2k_t \end{vmatrix}^T,$$

where L is the distance between A and B. The nodal forces in the coordinate directions can be determined by a simple transformation:

$$f_{xi} = F_{ni}\cos\theta - F_{ti}\sin\theta, \qquad f_{yi} = F_{ni}\sin\theta + F_{ti}\cos\theta, \tag{11, 12}$$

where $i = 1, 2, 3, 4$. Eliminating $\{U\}$ and $\{F\}$ from eqns (9)–(12), we obtain the nodal forces as a function of the nodal displacements in the coordinate direction

$$\{f\} = [ki]\{u\}, \tag{13}$$

where

$$\{f\} = \{f_{x1}, f_{y1}, f_{x2}, \ldots, f_{y4}\}^T,$$

and

$$[ki] = \frac{L}{6} \begin{vmatrix} 2A & 2C & A & C & -2A & -2C & -A & -C \\ & 2B & C & B & -2C & -2B & -C & -B \\ & & 2A & 2C & -A & -C & -2A & -2C \\ & & & 2B & -C & -B & -2C & -2B \\ & & & & 2A & 2C & A & C \\ & & & & & 2B & C & B \\ \text{symm.} & & & & & & 2A & 2C \\ & & & & & & & 2B \end{vmatrix},$$

in which $A = \alpha^2 k_n + \beta^2 k_t$, $B = \beta^2 k_n + \alpha^2 k_t$ and $C = \alpha\beta(k_n - k_t)$. Note that in the analysis,

we simplify the above relationship by letting k_n equal k_t. The stiffness matrix, $[ki]$, of each interface element needs to be generated at each step of an incremental loading path in the nonlinear finite element analysis. Moreover, when fiber/matrix debonding occurs, the stiffness of spring in the interface element is removed gradually over several load increments. This is due to the fact that, in a nonlinear analysis, the change has to be made gradually to obtain a convergent solution.

3.3. *Procedure for determining the local and overall properties*

For a state of uniform stress, the mechanical performance of a composite can be obtained through the following three steps:

(1) The composite unit cell is replaced by an equivalent homogeneous cell. For the boundary conditions at the vertices as shown in Fig. 2, the force, $\{\mathbf{f}\}$, at the vertices can be obtained as a function of the applied uniform stresses, $\{\sigma\}$, i.e.

$$\{\mathbf{f}\} = [R]\{\sigma\}, \tag{14}$$

where

$$\{\mathbf{f}\} = \{f_{x2}, f_{x3}, f_{y3}\}^T, \quad \{\sigma\} = \{\sigma_x, \sigma_y, \tau_{xy}\}^T,$$

and

$$[R] = \begin{vmatrix} \dfrac{1}{2\sqrt[4]{3}} & 0 & -\dfrac{\sqrt[4]{3}}{2} \\ \dfrac{1}{2\sqrt[4]{3}} & 0 & \dfrac{\sqrt[4]{3}}{2} \\ 0 & \dfrac{\sqrt[4]{3}}{2} & \dfrac{1}{2\sqrt[4]{3}} \end{vmatrix}.$$

(2) The resulting equivalent forces and the aforementioned boundary conditions are then applied to the composite unit cell. The local stress and strain fields and the displacements at the vertices of the composite cell are obtained from finite element analysis.

(3) The composite unit cell is again replaced by the equivalent homogeneous cell. For the same vertex boundary conditions as in step (1), the equivalent strain, $\{\varepsilon\}$, can be obtained as a function of the displacements at the vertices, $\{\mathbf{u}\}$, i.e.

$$\{\varepsilon\} = [R]^T\{\mathbf{u}\}, \tag{15}$$

where

$$\{\varepsilon\} = \{\varepsilon_x, \varepsilon_y, \gamma_{xy}\}^T, \qquad \{\mathbf{u}\} = \{u_2, u_3, v_3\}^T.$$

The result of $\{\varepsilon\}$ represents the overall transverse strain of the composite under the overall uniform transverse stress, $\{\sigma\}$.

4. NUMERICAL EXAMPLES AND DISCUSSION

The peformance of Kevlar/epoxy composite systems in the transverse direction is investigated. The Kevlar fiber is assumed to be transversely isotropic and linearly elastic. The epoxy matrix is assumed to be elastic–perfectly plastic. The mechanical properties of

Table 1. Fiber and matrix mechanical properties

Kevlar fiber	
Axial Young's modulus, E_A	126.7 GPa
Transverse Young's modulus, E_T	7.0 GPa
Axial shear modulus, G_A	3.0 GPa
Transverse shear modulus, G_T	2.692 GPa
Axial Poisson's ratio, ν_A	0.3
Transverse Poisson's ratio, ν_T	0.3
Epoxy matrix	
Young's modulus, E_m	3.0 GPa
Shear modulus, G_m	1.111 GPa
Poisson's ratio, ν_m	0.35
Yield stress, σ_y	70 MPa

Kevlar and epoxy are obtained from Tsai (1988) and listed in Table 1. Experimental results obtained from Pindera *et al.* (1987) show no evidence of matrix failure for the composite under transverse loadings. Therefore, the possibility of matrix failure is not considered in the analysis.

A limiting case, which assumes perfect bonding between the fiber and matrix, is studied first. The initial transverse Young's and shear moduli for Kevlar/epoxy composites with various fiber volume fractions (v_f) are determined and listed in Tables 2 and 3, respectively. The upper and lower bound solutions predicted by Hashin's (1979) and Teply and Dvorak's (1988) models are also listed in the Tables for comparison. It can be seen that the bounds are extremely close from both models and the present results are within the bounds.

As mentioned in the previous section, the interfacial shear debonding is not included in the analysis, since interfacial shear strength is usually much larger than interfacial tensile strength. Two interfacial tensile strengths ($\sigma_t \to \infty$ and $\sigma_t = 0$) are assumed in the next example. When $\sigma_t \to \infty$, perfect bonding is modeled. When $\sigma_t = 0$, any interfacial tensile stress will cause debonding. Consequently, no shear stress can be transmitted at the debonding region. The stress–strain curves for the Kevlar/epoxy composites with $v_f = 0.55$ under transverse tension, shear and compression are predicted. The results for both limiting cases are shown as solid lines in Figs 4–6 for tension, shear and compression, respectively.

As shown in Figs 4 and 5, the transverse tension and shear responses are very sensitive to the interfacial tensile strength. On the contrary, the compressive responses are very close

Table 2. Transverse Young's modulus (GPa) of Kevlar/epoxy composites with various fiber volume fractions

v_f	0.2	0.4	0.6	0.8
Hashin's model				
upper bound	3.872	4.522	5.232	6.019
lower bound	3.838	4.428	5.116	5.953
Teply and Dvorak's model				
upper bound	3.856	4.460	5.177	6.033
lower bound	3.800	4.386	5.087	5.943
Present model	3.838	4.434	5.140	5.980

Table 3. Transverse shear modulus (GPa) of Kevlar/epoxy composites with various fiber volume fractions

v_f	0.2	0.4	0.6	0.8
Hashin's model				
upper bound	1.313	1.571	1.872	2.223
lower bound	1.297	1.526	1.814	2.187
Teply and Dvorak's model				
upper bound	1.305	1.540	1.844	2.230
lower bound	1.280	1.506	1.799	2.182
Present model	1.297	1.529	1.826	2.202

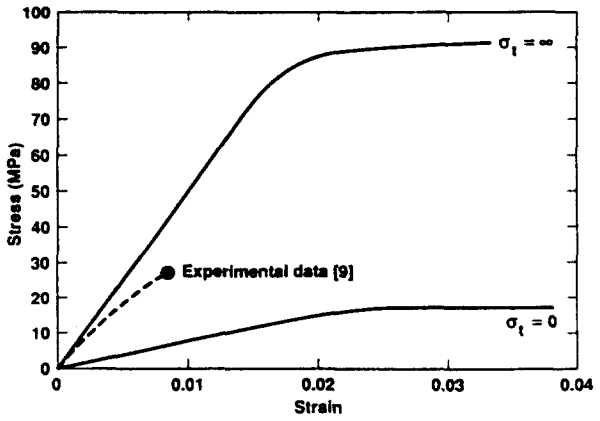

Fig. 4. Transverse tensile responses for the Kevlar/epoxy composite with $v_f = 0.55$.

for both limiting cases. Experimental data obtained from Pindera *et al.* (1987) are also plotted as dashed lines in Figs 4–6 for comparison. It can be seen that good agreement is obtained for the initial moduli by assuming perfect bonding. The experimental results of transverse tension and shear are bounded by the two limiting cases. Although the experimental compressive response is not bounded by the limiting cases, the difference is small. This difference may be caused by the fact that epoxy material has a slight material hardening effect, which is not included in the analysis.

More calculations are conducted for the same composite system with various interfacial tensile strengths. The predicted ultimate composite strengths as a function of the interfacial

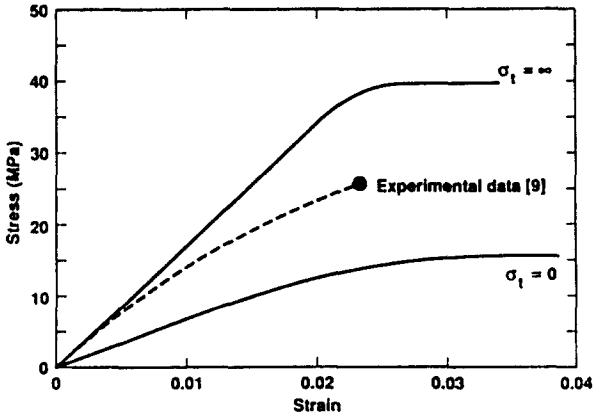

Fig. 5. Transverse shear responses for the Kevlar/epoxy composite with $v_f = 0.55$.

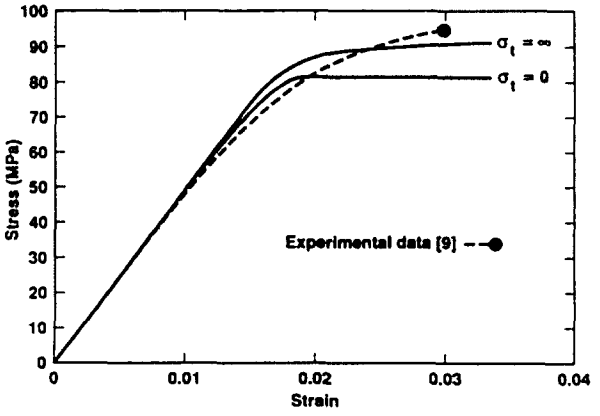

Fig. 6. Transverse compressive responses for the Kevlar/epoxy composite with $v_f = 0.55$.

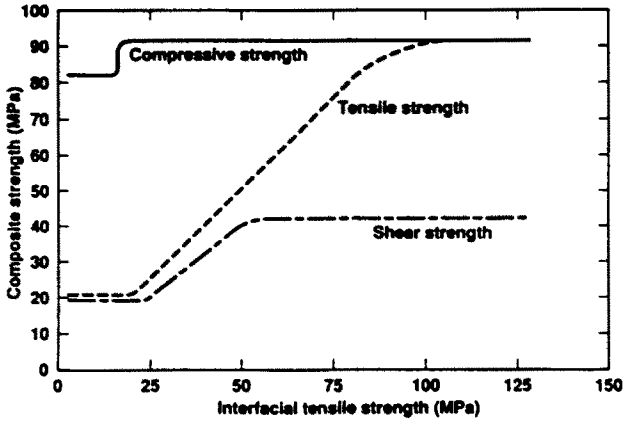

Fig. 7. Predicted ultimate composite strength as a function of interfacial tensile strength for the Kevlar/epoxy composite with $v_f = 0.55$.

tensile strength (σ_t) are shown in Fig. 7. The curves can be divided into three regions. The plateau region at the higher values of σ_t indicates that no debonding will occur before the final failure. In the plateau region at the lower values of σ_t, more load can be carried by the composite after debonding. In the region between these two plateau regions, the final failure will occur immediately upon debonding. Note that the analysis predicts two types of stress–strain curves. In the two plateau regions shown in Fig. 7, the composites exhibit one type of stress–strain curve, which is similar to the stress–strain curves for the cases $\sigma_t \to \infty$ and $\sigma_t = 0$ shown in Figs 4–6. These stress–strain curves have a plateau region and the overall stress is almost a constant in this region. This constant is treated as the ultimate strength for the composite with this stress–strain plateau. Between those two plateau regions, the composites exhibit the other type of stress–strain curve. In this case, a sudden drop in stress due to debonding appears in the stress–strain curve and the maximum stress is taken as the ultimate strength of the composite.

In the last example, the Kevlar/epoxy composite with $v_f = 0.55$ is studied under overall combined transverse loadings (σ_x and τ_{xy}). The ultimate composite strength is determined from this analysis for four values of interfacial tensile strength (0 MPa, 25 MPa, 50 MPa, ∞). By connecting the ultimate strengths for each σ_t, failure envelopes are obtained and plotted in Fig. 8. It is not surprising to see that the interfacial tensile strength has more pronounced influence on the tensile and shear strengths than the compressive strength. Also note that the shapes of failure envelopes are quite different from the ellipses predicted by the Tsai–Wu (1971) failure criterion.

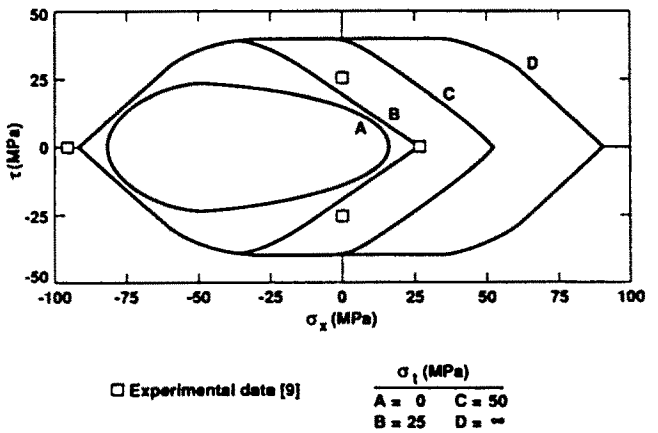

Fig. 8. Predicted failure envelope for the Kevlar/epoxy composite with $v_f = 0.55$ under biaxial loadings.

It can also be seen from Fig. 8 that the results of the present analysis are dependent on the assumed interfacial tensile strengths. For comparison, the experimental results obtained from Pindera *et al.* (1987) are also shown in the figure. We can see that both results are in close agreement for $\sigma_t = 25$ MPa. This agreement serves as an experimental verification of the interfacial tensile strength.

5. CONCLUSIONS

A finite element model employing special interface elements has been developed to study the effect of interface bond strength on the transverse behavior of the composites. The results show that the interfacial tensile strength has a significant influence on the transverse properties of Kevlar/epoxy composites. The present model can be used as a design tool to select interface bond strength in a binary composite under specific applied loads before the composite is manufactured.

Residual thermal stress is usually present at the interface with the composite due to the cooling processing temperature. For the composite studied here, the values of transverse thermal expansion coefficients for fiber and matrix are very close. Therefore, the transverse residual thermal stress is not included in the analysis. But if necessary, the residual thermal effects can easily be incorporated in this finite element model.

Note that since the periodic distribution of fibers is assumed in the model, the effect of fiber clustering is not included in the analysis. Consequently, the observation that transverse cracks are usually nucleated in regions where the fibers are more closely spaced and also propagate preferentially through such regions cannot be obtained from the analysis. This clustering effect is being studied using random fiber disributions. Also, note that the interface element developed in this study can be extended to include the effect of fiber–matrix slipping based on the Coulomb friction law.

Acknowledgements—The author acknowledges the discussion of the work with E. F. M. Winter and J. R. Brockenbrough.

REFERENCES

Adams, D. F. and Tsai, S. W. (1969). The influence of random filament packing on the transverse stiffness of unidirectional composites. *J. Comp. Mater.* **3**, 368–381.

Chou, T. W., Nomura, S. and Taya, M. (1980). A self-consistent approach to the elastic stiffness of short-fiber composites. *J. Comp. Mater.* **14**, 178–188.

Hashin, Z. (1979). Analysis of properties of fiber composites with anisotropic constituents. *J. Appl. Mech.* **46**, 543–550.

Hill, R. (1964). Theory of mechanical properties of fiber-strengthened materials—I. Elastic behavior. *J. Mech. Phys. Solids* **12**, 199–212.

Oshima, N. and Nomura, S. (1985). A method to calculate effective modulus of hybrid composite materials. *J. Comp. Mater.* **19**, 287–293.

Pindera, M. J., Gurdal, Z., Hidde, J. S. and Herakovich, C. T. (1987). Mechanical and thermal characterization of unidirectional aramid/epoxy. Report No. CCMS-86-08, VPI-E-86-29. Virginia Polytechnic Institute and State University.

Takahashi, K. and Chou, T. W. (1988). Transverse elastic moduli of unidirectional fiber composites with interfacial debonding. *Metall. Trans.* A **19A**, 129–135.

Teply, J. L. and Dvorak, G. J. (1988). Bounds on overall instantaneous properties of elastic–plastic composites. *J. Mech. Phys. Solids* **36**, 29–58.

Tsai, S. W. (1988). *Composites Design* (4th edn). Think Composites, Dayton OH.

Tsai, S. W. and Wu, E. M. (1971). A general theory of strength for anisotropic materials. *J. Comp. Mater.* **5**, 58–80.